ACS Photonics

Article

Cite This: ACS Photonics 2019, 6, 994−1001

pubs.acs.org/journal/apchd5

Single-Crystalline Gold Nanodisks on WS_2 Mono- and Multilayers for Strong Coupling at Room Temperature

Mathias Geisler,[†,‡] Ximin Cui,[§] Jianfang Wang,[§] Tomas Rindzevicius,[∥,⊥] Lene Gammelgaard,[‡,#] Bjarke S. Jessen,[‡,#] P. A. D. Gonçalves,[†,‡,○] Francesco Todisco,[○] Peter Bøggild,[‡,#] Anja Boisen,[∥,⊥] Martijn Wubs,[†,‡] N. Asger Mortensen,[‡,○,□] Sanshui Xiao,[†,‡] and Nicolas Stenger*[,†,‡]

[†]Department of Photonics Engineering, [‡]Center for Nanostructured Graphene, [∥]Department of Health Technology, [⊥]DNRF and Villum Fonden Center for Intelligent Drug Delivery and Sensing Using Microcontainers and Nanomechanics, and [#]Department of Physics, Technical University of Denmark, DK-2800 Kgs. Lyngby, Denmark

[§]Department of Physics, The Chinese University of Hong Kong, Shatin, Hong Kong SAR, China

[○]Center for Nano Optics and [□]Danish Institute for Advanced Study, University of Southern Denmark, DK-5230 Odense M, Denmark

Supporting Information

ABSTRACT: Engineering light−matter interactions up to the strong-coupling regime at room temperature is one of the cornerstones of modern nanophotonics. Achieving this goal could enable new platforms for potential applications such as quantum information processing, quantum light sources, and even quantum metrology. Layered materials like transition metal dichalcogenides (TMDCs) and, in particular, tungsten disulfide (WS_2), possess strong dipole moments which are comparable to semiconductor-based quantum dots, but the former also exhibit large exciton binding energies, thereby making TMDCs suitable candidates for exploring light−matter interactions at ambient conditions. Furthermore, the combination of TMDCs with plasmonic nanocavities, which tightly confine light down to nanometer scale, has recently emerged as a suitable platform for achieving strong coupling between plasmons and excitons at room temperature. Here, we use ultrathin single-crystalline gold nanodisks featuring large in-plane electric dipole moments aligned with the exciton's dipole moments in monolayer WS_2. By performing both scattering and reflection spectroscopy, we demonstrate strong coupling at room temperature with a Rabi splitting of ∼108 meV. In addition, when the plasmonic resonance of these nanodisks is coupled with few-layer WS_2, a Rabi splitting of ∼175 meV is observed, with a major increase of 62% relative to the monolayer configuration. Our results therefore suggest that ultrathin single-crystalline gold nanodisks coupled to WS_2 constitute an attractive platform to explore light−matter interactions in the strong-coupling regime.

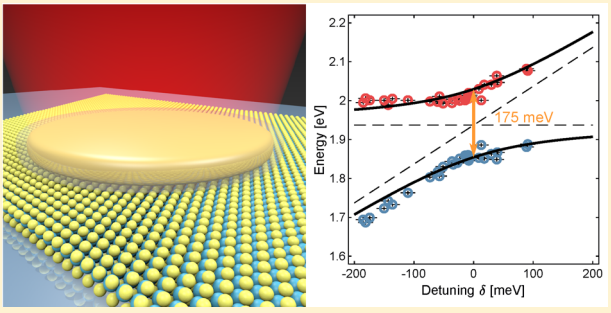

KEYWORDS: *plasmonics, TMDC, WS_2, strong coupling, excitons, gold nanodisks*

Efficient coupling between light and matter is important for many applications as well as for fundamental research within the field of nanophotonics. When the exchange rate of energy between an emitter and a cavity exceeds their intrinsic dephasing rates, the system enters the strong−coupling regime where new hybrid eigenstates form that are part light and part matter.[1] Reaching the strong-coupling limit in different systems has, for instance, enabled studies of quantum electrodynamics,[2] the experimental realization of low-threshold lasers,[3] and coupling a single quantum of energy to nitrogen-vacancy centers in diamond.[4,5] However, these investigations all required low temperatures to keep the emitter dephasing or the energy dissipation rate sufficiently low in order to achieve strong coupling.

The transition into the strong-coupling regime is dependent on the ability to control the coupling rate, g, between the emitter and the cavity. Since $g \propto \mu_{ex}\sqrt{N/V}$,[6] where μ_{ex} is the emitter's dipole moment strength, N is the number of emitters coherently coupled to the cavity, and V is the cavity (effective) mode volume, several key factors can be engineered in order to facilitate this transition. For purely dielectric cavities, the typical mode volume is on the order of $(\lambda/n)^3$ due to the diffraction limit, thereby limiting the maximum attainable coupling strength and requiring long coherence times for both the cavity and the emitter states in order to enter the strong−coupling regime. On the other hand, plasmonics offers the possibility of subwavelength mode volumes, with associated strong enhancement of the field strength, albeit at the price of

Received: December 22, 2018
Published: March 28, 2019

DOI: 10.1021/acsphotonics.8b01766
ACS Photonics 2019, 6, 994−1001

higher losses, mainly due to absorption in the metal.[7] In the latter context, coupling plasmons to various organic and inorganic semiconductors has gained increasing attention in recent years,[8−14] and plasmonic systems have been employed to reach the strong-coupling regime when interacting with organic molecules,[6,15−18] resulting in enhanced nonlinearities and low-threshold polariton lasing and condensation.[19,20]

Moreover, excitons in two-dimensional (2D) materials and, in particular, in TMDC monolayers and respective multilayers have been the object of an intense study in recent years, partly due to their unique optical properties,[21] capable of merging together the main properties of Frenkel excitons in organic semiconductors (high binding energy and large oscillator strength) with that of Wannier−Mott excitons in inorganic quantum wells (relatively large exciton radius, low photodegradation, and small saturation density) at room temperature.[21] Examples of studies demonstrating strong coupling with excitons in 2D materials, both at cryogenic and room temperature, include, for instance, excitons in TMDCs coupled to plasmonic lattices,[22,23] plasmonic and dielectric cavities,[12,24−29] or to individual plasmonic nanoparticles.[30,31] Some studies have even reported coupling to charged excitons (trions) in WS_2,[32] as well as self-hybridization of the excitons with cavity modes in many-layer TMDC systems.[33−35] The lattice structure of the TMDCs furthermore gives rise to a new degree of freedom in the form of valley polarization, which can be addressed using circularly polarized light when coupled to plasmonic structures.[36,37]

In this work, we report the observation of the strong coupling between localized surface plasmons supported by high-quality, single-crystalline gold nanodisks, and excitons in mono- and multilayer WS_2. Both systems exhibit strong in-plane optical responses, and by controlling the nanoparticles' size we achieve spectral and spatial overlap between the dipolar plasmon mode of the nanodisks and the *A*-exciton of WS_2.[38,39] Due to the high aspect ratio and quality of our single-crystalline gold nanodisks, we were able to experimentally observe strong plasmon-exciton coupling in both scattering and reflection measurements, characterized by a Rabi splitting of 108 ± 8 meV at room temperature. Motivated by a recent work,[31] we also show that when substituting the WS_2 monolayer with a multilayer (seven layers in our case), an increase in the Rabi splitting to 175 ± 9 meV is observed. To the best of our knowledge, this is the highest Rabi splitting reported for layered TMDCs coupled to an open plasmonic cavity. The accessibility of the open cavity, along with the clear presence of the strong-coupling regime, is an important stepping stone toward a further study of the plethora of fundamental physics in these strongly coupled light−matter systems, along with potential applications in quantum information processing, quantum metrology, nonlinear optical materials, and quantum light sources.

RESULTS AND DISCUSSION

We investigate strong plasmon−exciton coupling at room temperature by depositing ultrathin single-crystalline gold nanodisks on monolayers of WS_2, as depicted in Figure 1a. Such plasmonic nanodisks were chosen due to their strong in-plane dipole mode associated with the dipolar localized surface plasmon resonance (LSPR); these are tunable by controlling the nanodisk's radius (on the order of 30 nm)[38] and exhibit narrow line widths due to the single-crystalline nature of the nanodisks. Moreover, like the other 2D TMDCs, WS_2 has a

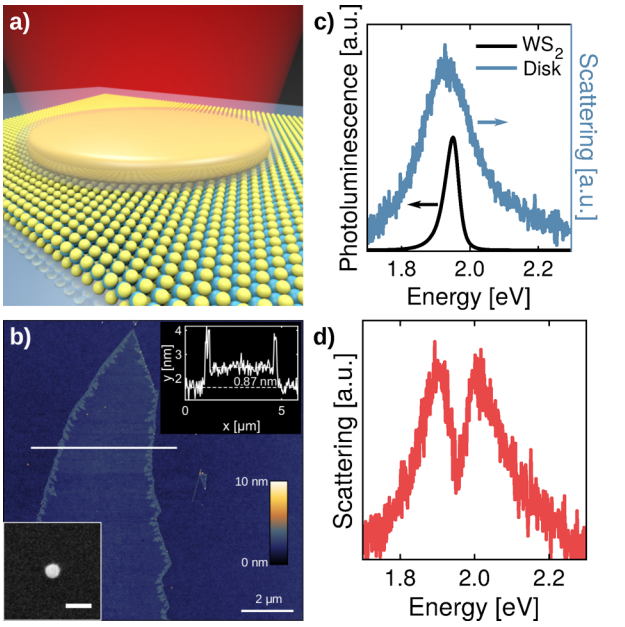

Figure 1. (a) Sketch of a single-crystalline gold nanodisk coupled to monolayer WS_2. (b) Atomic force microscopy image of a monolayer WS_2 flake. The inset in the upper right corner shows the height profile along the white line, while the one in the lower left corner shows a scanning electron microscopy image of a typical nanodisk. Scale bar is 100 nm. (c) Photoluminescence spectrum of monolayer WS_2 (black) and dark-field scattering spectrum of an individual, uncoupled nanodisk (blue). (d) Experimental scattering spectrum of a single nanodisk coupled to WS_2 clearly showing the splitting between the upper and lower polariton branch.

strong in-plane excitonic response, characterized by a large transition-dipole moment.[10,40,41] This, together with the stability of excitons in atomically thin WS_2 (owing to their large binding energies[42]), makes our system extremely well-suited for exploring light−matter interactions in the strong-coupling regime at room temperature.

Flakes of WS_2 were mechanically exfoliated from commercially available bulk crystals (HQ Graphene) onto plasma cleaned SiO_2/Si substrates. Monolayer flakes were automatically detected and identified by quantitative optical mapping.[43] The monolayer nature of these flakes was further confirmed by atomic force microscopy (AFM), see Figure 1b, where the height of the flake was found to be ≈0.87 nm, in agreement with previously reported results.[39] The photoluminescence (PL) spectrum, represented by the black line in Figure 1c, reveals the exciton emission, where the asymmetry of the peak to the low-energy side is caused mainly by the interaction with phonons.[44] From this spectrum we find an emission energy of $E_{em,ex}$ = 1.951 eV, in accordance with the literature[39] (for more information, see Figure S1).

To extract the energy and corresponding line width associated with the optical transition of the *A*-exciton, we performed reflection measurements on five different monolayer flakes, using spatially filtered white light to ensure normal incidence. Employing the transfer-matrix method[45,46] we retrieved the WS_2 dielectric function for each flake, from which we extract an average exciton energy E_{ex} = 1.963 eV and line width Γ_{ex} = 28 meV; see Figure S2 and Table S1 in the Supporting Information.

The open plasmonic cavities used in this work consist of cylindrical single-crystalline gold nanodisks, chemically synthe-

DOI: 10.1021/acsphotonics.8b01766
ACS Photonics 2019, 6, 994−1001

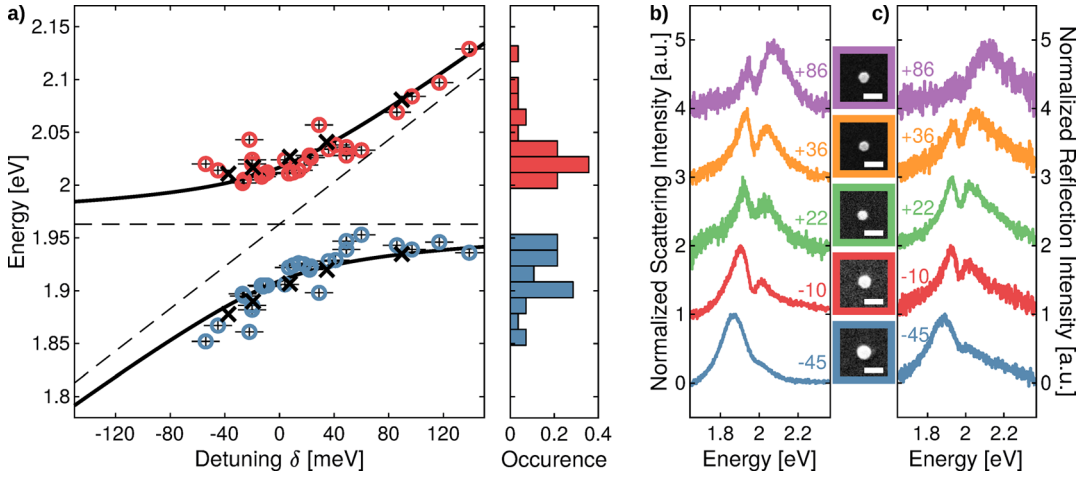

Figure 2. (a) Dispersion retrieved from scattering measurements of the coupled plasmon−exciton system, consisting of single-crystalline gold nanodisks on monolayer WS_2, with the lower (blue) and upper (red) polariton branch. The right panel shows the distribution of the measured peaks. The solid black line corresponds to a fit to the data using eq 2, while the horizontal and sloped dashed lines indicate the exciton and plasmon energies, respectively. The black crosses are the peak positions extracted from the theoretically calculated spectra plotted in Figure 3b. (b) Experimental dark-field scattering spectra from five different individual gold nanodisks demonstrating the evolution of the optical response with different plasmon energies. The individual detunings $\delta = E_{pl} - E_{ex}$ are presented next to the corresponding spectra. (c) Measured reflection spectra for the same five particles, as in (b). The absorption of the disks dominates the extinction spectra by more than an order of magnitude making the reflection spectrum representative of the absorption (see Figure 3a). The insets are scanning electron microscope images of the five gold nanodisks; the scale bar is 100 nm.

sized as described in ref 38. Briefly, triangular gold nanoplates were first synthesized using a three-step seed-mediated method.[47] The nanodisks were produced by performing anisotropic oxidation on the nanoplates. The oxidation allows for finely tailoring the nanodisk diameter, and the thickness of the gold nanodisks remained unchanged during the oxidation process. A thin layer (∼1 nm) of cetyltrimethylammonium bromide (CTAB) is present on the surface of the nanodisks after the synthesis.[38] In our study, cylindrical gold nanodisks of 8.8 ± 0.2 nm in thickness, measured without the CTAB layer, were chosen because of their moderate plasmon damping and concomitant narrow plasmon line width. Due to the inherent variation in particle radii, each batch contains particles with their LSPRs distributed around a mean energy, the latter chosen to match the exciton energy (E_{ex} = 1.963 eV). A representative scattering spectrum of a single gold nanodisk is shown in Figure 1c. Measuring the uncoupled nanodisks on the bare SiO_2/Si substrate results in an average line width of the plasmon resonance of Γ_{pl} = 170 meV. The variation of the particles' LSPRs is exemplified in ensemble measurements performed on the nanodisk solution in Figure S3, where the extinction spectra show a width about twice that of the individual nanodisks due to inhomogeneous broadening. For a resonant energy around 1.96 eV we obtain a Q-factor of $E_{pl}/\Gamma_{pl} \approx 11.5$, close to its intrinsic quasi-static limit of ∼13.5 for an arbitrarily-shaped gold nanoparticle when only the dielectric function is considered.[48] This shows that other dissipation pathways, such as surface scattering and disorder, are minimized due to the single-crystalline nature of the nanodisks.

Reaching the strong-coupling regime requires a simultaneous spatial and spectral overlap of the LSPR and the exciton in the nanodisk and WS_2, respectively. The spatial overlap was ensured by dropcasting the nanodisks directly onto the WS_2 flakes. The CTAB molecule layer ensures a narrow gap without direct contact between the metal and the underlying flake in order to prevent possible quenching. As mentioned above, the spectral overlap was ensured by selecting the appropriate nanodisk's radius. Moreover, in 2D TMDCs, the dipole moment of the exciton is strongly oriented in the plane of the 2D layer,[41] which requires special attention when coupling to external fields. However, the dipolar LSPR mode of the nanodisk is oriented in the same plane as the excitons, thus, promoting a strong interaction.[38] Finite-element and analytic calculations corroborate the observed resonance energy of the nanodisks even in the presence of a high-refractive index material, such as WS_2, underneath (see Figure S4). The inherent size distribution (with different radii) in a batch of gold nanodisks straighforwardly enables measurements on different nanodisks, with LSPRs distributed around the energy of the exciton (thereby allowing us to study the light−matter interaction at positive and negative detunings). Using dark-field (DF) microscopy, we then obtained scattering spectra for each individual particle. In addition to the DF measurements, scanning electron microscope images were taken to ensure that the acquired spectra originated only from single nanodisks rather than from dimers or particles with other morphologies. Due to the small size and correspondingly small scattering efficiency of the nanodisks, careful background removal was key to isolating the signal of the coupled system. This background was caused by scattered light from nearby WS_2 edges as well as exciton photoluminescence (see Supporting Information for further details). A typical spectrum taken from a gold nanodisk resting on a WS_2 monolayer is shown in Figure 1d, where two distinct peaks appear around the bare exciton energy. The almost equal strength of the two peaks indicates that the LSPR of the nanodisk is close to the exciton resonance. By measuring particles with different radii and, thus, different LSPR energies, we are in this manner able to map out the dispersion of the coupled system as a function of the plasmon−exciton energy detuning. All the acquired spectra show a double-peaked line shape. Extracting the energy of the peaks from the scattering spectra, a clear anticrossing behavior is observed, as shown in Figure 2a, which is a hallmark of these emitter−cavity coupled systems.[1,17,18]

DOI: 10.1021/acsphotonics.8b01766
ACS Photonics 2019, 6, 994−1001

In order to analyze the data, we apply the coupled-oscillator model (COM) in its non-Hermitian Hamiltonian form given by the eigenvalue problem:[49]

$$\begin{bmatrix} E_{pl} - i\frac{\Gamma_{pl}}{2} & g \\ g & E_{ex} - i\frac{\Gamma_{ex}}{2} \end{bmatrix} \begin{bmatrix} \alpha \\ \beta \end{bmatrix}_{\pm} = E_{\pm} \begin{bmatrix} \alpha \\ \beta \end{bmatrix}_{\pm} \quad (1)$$

where $E_{pl(ex)}$ and $\Gamma_{pl(ex)}$ are the plasmon (exciton) energy and line width, respectively, g is the coupling strength, and α and β are the amplitudes describing the polaritonic state in terms of its plasmonic ($\alpha_{\pm}$) and excitonic ($\beta_{\pm}$) constituents. Diagonalizing the Hamiltonian yields the two energy eigenvalues

$$E_{\pm} = \frac{1}{2}(E_{pl} + E_{ex}) - \frac{i}{4}(\Gamma_{pl} + \Gamma_{ex}) \pm \frac{1}{2}\sqrt{4g^2 + \left[\delta - \frac{i}{2}(\Gamma_{pl} - \Gamma_{ex})\right]^2} \quad (2)$$

where we have introduced the plasmon-exciton detuning, $\delta = E_{pl} - E_{ex}$. The eigenvalues describe an energy spectrum divided into an upper polariton branch (UPB, E_+) and a lower polariton branch (LPB, E_-). The Rabi splitting E_{Rabi} is then defined as the energy difference between the UPB and LPB at zero detuning,[8] giving

$$E_{Rabi} = \sqrt{4g^2 - \frac{(\Gamma_{pl} - \Gamma_{ex})^2}{4}} \quad (3)$$

From the scattering spectra of the individual nanodisks on WS_2, we extracted the respective energies of the upper and lower polariton branches, E_+ and E_-. From energy conservation, we then obtained the plasmon energy as $E_{pl} = E_+ + E_- - E_{ex}$. The avoided crossing is clearly visible from the histogram in the right side of Figure 2a, with no data points located between the two polaritonic branches. The vertical error bars represent the uncertainty associated with the extracted peak positions, which we estimate to be on the order of ±5 meV. The horizontal error bars represent the propagated uncertainties in the calculated detunings, which are dominated by the standard deviation of the measured exciton energy.

To estimate the coupling strength g and the Rabi splitting E_{Rabi}, we simultaneously fit the real part of the eigenvalue spectrum (eq 2) to the experimentally determined dispersion of the UPB and LPB. In the fitting procedure, we fix the values of the exciton energy (E_{ex} = 1.963 eV), the exciton line width (Γ_{ex} = 28 meV), and the plasmon line width (Γ_{pl} = 170 meV) to the experimentally determined values, which leaves the coupling strength as the only free parameter. The g-value found in this manner represents an ensemble average of the system, in general, as variations in particle size and the local environment can influence the number of participating excitons and through that the individual coupling strengths (see the Supporting Information for further discussion). The described procedure yields a value of g = 64 ± 3 meV, from which we calculate a Rabi splitting of E_{Rabi} = 108 ± 8 meV using eq 3. Comparing this with the overall losses in the system $\frac{1}{2}(\Gamma_{pl} + \Gamma_{ex})$ = 99 ± 3 meV, we see that our hybrid nanodisk/WS_2 system is just at the onset of the strong-coupling regime, as per the criterion $E_{Rabi} > \frac{1}{2}(\Gamma_{pl} + \Gamma_{ex})$.

Five selected scattering spectra showing the evolution of the optical response of the hybrid system are depicted in Figure 2b. The figure clearly shows an avoided crossing in the succession of the individual spectra, together with a shift of spectral weight from the LPB to the UPB as the detuning approaches δ = 0 meV from below. In addition, we note that the noise generally increases for larger positive δ since the LSPR energy increases with decreasing particle radius, resulting in a lower scattering cross section.

Since $\delta = E_+ + E_- - 2E_{ex}$, the exact value for δ reported in Figure 2b,c is highly sensitive to the value of E_{ex}. From the reflection measurements on the bare WS_2 flakes alone, we observe exciton energies in the range 1.958 to 1.968 eV, corresponding to a detuning variation of $\Delta\delta$ = 20 meV, which may influence the COM fit. Therefore, we also use the COM to extract the peak positions associated with the UPB and LPB, and also to obtain the exciton energy,[50] see Figure S8. From this approach, we find a slightly higher average, exciton energy of E_{ex} = 1.981 eV, but also a larger spread of 40 meV (i.e., $\Delta\delta$ = 80 meV). This larger variation and change in E_{ex} (with respect to the same quantity measured prior to the nanodisks' deposition) can be caused by, for instance, local strain or induced doping from the nanoparticle solution.[51] Nevertheless, using instead this averaged E_{ex} in the same analysis as before results in a change of only 4 meV in the obtained Rabi splitting, despite the shift of 36 meV in the detuning for all measurement points, see Figure S9.

The strong-coupling regime is associated with a pronounced mode splitting not only in the scattering but also in the absorption spectrum of the coupled system.[52] Often, the presence of the splitting in absorption is only verified numerically,[30,31] since measuring the absorption independently from the scattering normally requires specialized techniques.[53]

We address this by performing bright-field reflection measurements on the same samples. Due to their morphology, the raw reflection spectrum, $\mathcal{R}_{raw}$, contains both scattering and absorption contributions from the coupled system, as well as the strong absorption lines of the excitons in the uncoupled WS_2, $\mathcal{R}_{WS_2}$. However, our nanodisks have small radii (<35 nm) and a thickness of only 8.8 nm, and numerical calculations suggest that the absorption cross section is larger than the scattering cross section by more than an order of magnitude (cf. Figure 3a). As such, the raw reflection spectrum will contain information about the absorption properties of the coupled nanodisk/WS_2 system.

In order to isolate this information, careful background removal is required. We therefore calculate the coupled nanodisk/WS_2 reflection spectrum as

$$\Delta\mathcal{R} = \frac{\mathcal{R}_{WS_2} - \mathcal{R}_{raw}}{\mathcal{R}_{sub}} \quad (4)$$

where $\mathcal{R}_{sub}$ is the reflection from the bare SiO_2/Si substrate. This normalization takes into account the substrate contribution (for further details, see the Supporting Information). The reflection spectra calculated in this manner from the same five particles as in Figure 2b are shown in Figure 2c. As E_{pl} is tuned across the exciton energy, we observe a similar behavior in reflection as for the scattering spectra. We note that the absorption is blueshifted in all cases when compared to the scattering, which is also observed in our calculations; cf. Figure 3b,c.[54] The observation of mode splitting and hybridization not only in scattering, but also in the reflection spectra further supports and corroborates our observation of the strong coupling in our nanodisk/WS_2 system.

In addition to the experiments, we perform finite-element method (FEM) calculations of the electrodynamics governing the system's response (see Methods). In the computations, we

DOI: 10.1021/acsphotonics.8b01766
ACS Photonics 2019, 6, 994−1001

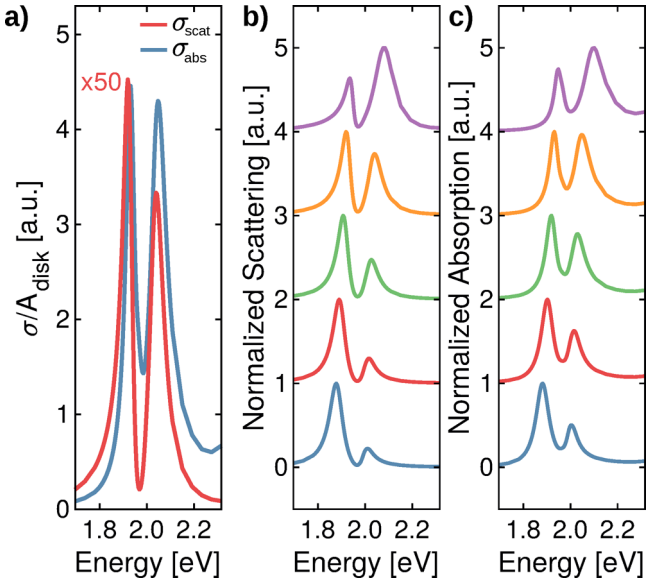

Figure 3. (a) Calculated scattering (red) and absorption (blue) cross sections σ obtained with finite-element method calculations of a nanodisk of radius R = 23 nm normalized to the geometrical area. The scattering cross section has been multiplied by 50 to match the scale. The ratios between the maxima of σ_{abs} and σ_{scat} vary from 96 (R = 19 nm) down to 21 (R = 29 nm). (b, c) Normalized scattering and absorption of particles of radii R = 19, 23, 25, 27, and 29 nm, arranged from top to bottom.

take the experimentally determined radii (from 19 to 29 nm)[38] and nanodisk thickness (9 nm), as well as a 1 nm thick polymer layer surrounding the particle. We furthermore use our experimentally determined dielectric function of the WS_2 flakes; see Supporting Information. For optical constants of gold, we use the values of McPeak et al.[55] in optimized film quality conditions. This choice of reference data was made to better reflect the single-crystalline nature of our nanodisks. In this way, we obtain scattering and absorption spectra of the particles, as shown in Figure 3b,c. Since the nanodisks are thinner than the skin depth of gold of around 25 nm at 1.96 eV,[56] the electric field completely permeates the particles, making the results very sensitive to the particular value of the dielectric function. For instance, using instead the values from Johnson and Christy[57] redshifts the resonance position by around 40 meV (see Figure S12), and changes in especially the imaginary part of ε have been reported for thin gold films.[58] However, we still see that we are able to reproduce the experimentally observed behavior both in scattering and absorption with good agreement. The calculations show scattering cross sections approaching zero at the exciton's energy, indicative of strong plasmon−exciton coupling.[52] These same near-zero intensities are not observed in the experiments, which may be caused by a background signal coming from the strong scattering from the WS_2 flake edges. Although we perform background removal on all measured spectra, the scattering cross section of the nanodisks is small and any remaining background is expected to influence the overall signal intensity. Note, however, that in the calculated absorption spectra, these same near-zero intensities are not observed due to power dissipated within the WS_2.[18,52]

Extracting the peak locations of the calculations in the same fashion as for the experimental results allows us to compare the positions of the UPB and LPB to the experimental data, as indicated by the black crosses in Figure 2a, thereby showing an excellent agreement between the experiment and the numerical calculations.

Besides studying strong coupling between the LSPRs supported by the nanodisks and the excitons in monolayer WS_2, we have also performed measurements with few-layer WS_2. Recent experiments[27,31,59] have reported the possibility of increasing the mode splitting by increasing the number of TMDC layers coupled to the plasmonic resonator. In order to assess the magnitude of this effect in our system, we have measured the optical response of the gold nanodisks on a WS_2 flake 4.4 nm in height, which corresponds to seven layers. Using the transfer-matrix method as before, we extract the dielectric function of the multilayer WS_2 flake, which is dominated by a main excitonic resonance at $E_{ex,multi}$ = 1.942 eV, with a line width of $\Gamma_{ex,multi}$ = 44 meV (see Table S2). We note that both the broadening and redshift of the A-exciton resonance are well-known for multilayers.[31] Following the same procedure for data analysis as in the monolayer case, we have obtained the results plotted in Figure 4, exhibiting a

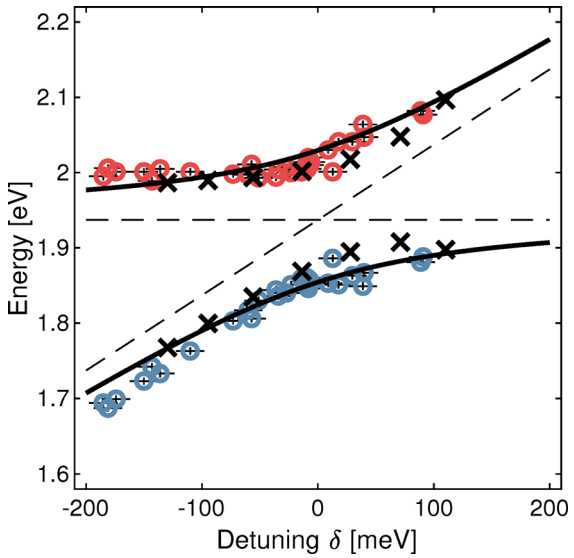

Figure 4. Experimentally obtained dispersion for the coupled plasmon-exciton system on multilayer WS_2. Note the change in scale of the y-axis compared to Figure 2a.

pronounced avoided crossing akin to the strong-coupling phenomena. In the multilayer configuration, we observe a 45% increase of the coupling strength, resulting in g_{multi} = 93 ± 4 meV, which in turn is associated with a Rabi splitting of $E_{Rabi,multi}$ = 175 ± 9 meV, corresponding to a remarkable 62% increase. To the best of our knowledge, this is the highest Rabi splitting reported in a TMDC coupled to an open plasmonic cavity.[28,30,31,60] Furthermore, the direct availability of the open plasmonic cavity is advantageous for future near-field explorations and sensing applications, as well as external coupling to other cavities and optical circuit elements, when compared to closed-cavity configurations.[33,35,61]

In order to understand the increase in the coupling strength that we observe for the seven-layer WS_2 flake, we have performed numerical calculations using the dielectric function extracted from our reflection measurements. The ensuing positions of the UPB and LPB are indicated by the black crosses in Figure 4. The calculations predict an overall increase

DOI: 10.1021/acsphotonics.8b01766
ACS Photonics 2019, 6, 994−1001

of the coupling strength with the number of layers. However, quantitatively, we observe a slightly lower increase in the Rabi splitting in comparison to our experimental data. This difference could be due to the fact that we have approximated the optical response of multilayer WS_2 as an isotropic dielectric function, and we therefore do not take into account the out-of-plane response of multilayer WS_2. Despite these quantitative differences, we observe qualitative agreement between our calculations and our experimental data. We explain this significant increase in the Rabi splitting with an increased number of excitons participating in the coupling. Furthermore, our numerical calculations suggest that additional layers will not increase the coupling strength substantially, since we observe an exponential decay of the plasmon mode energy to $1/e$ inside the WS_2 over a length of ∼4 layers (see Figure S13). These conclusions are in agreement with recent experimental works,[27,31] although we emphasize that the saturation effect appears to be system-dependent.[59]

CONCLUSION

We have experimentally demonstrated strong coupling between single-crystalline, high-aspect ratio gold nanodisks on mono- and multilayers of WS_2 at room temperature. In the monolayer case, we extract a Rabi splitting of 108 ± 8 meV (g = 64 ± 3 meV). Additionally, we have observed the strong coupling both in scattering and reflection measurements, where the latter is indicative of the coupled system absorption. In the multilayer configuration, we achieved a significant 62% increase of the Rabi splitting to 175 ± 9 meV (g_{multi} = 93 ± 4 meV), that is, in excess of six times k_BT at room temperature. The increase is enabled by a larger mode overlap of the plasmon field and the WS_2.

This way of controlling the coupling regime in plasmonic nanodisks and structurally similar systems is a key component toward applications within all-optical circuitry, polaritonic lasers, and quantum information processing, as well as the exploration of possible antibunching effects in multiple emitters coupled to plasmonic cavities.[13,62]

METHODS

Optical Measurements. A custom spectroscopy setup built from a Nikon Eclipse Ti−U inverted microscope was used for the optical measurements. For the dark-field and bright-field spectra, a halogen lamp with a tunable power up to 100 W was used, while for the photoluminescence, a 407 nm diode laser (Integrated Optics) was used. The light was focused on the sample with a TU Plan Fluor objective from Nikon (100×, 0.9 NA) and collected with the same objective. Afterward, the light was directed toward a slit, allowing for a precise selection of the collection area. The light then entered a Shamrock 303i spectrometer equipped with a 450 nm long-pass filter (FELH0450 from Thorlabs) and an electronically cooled Newton 970 EMCCD for acquiring spectra. All spectra consist of the sum of several lines on the 2D CCD uniquely identified for each particle. Each of these spectra were first corrected for dark counts and then for background using the local environment in close vicinity of the individual particles obtained directly from the same spectroscopic image. Finally, the spectra were divided by the normalized white light spectrum of the halogen lamp. The photoluminescence spectra were obtained in a similar manner, apart from the white light spectrum correction. All experiments were performed at room temperature.

Finite-Element Calculations. A commercially available FEM software (COMSOL Multiphysics v. 5.3a) was used to compute the electrodynamic response of the gold nanodisks placed on top of the mono- and multilayer WS_2. We have performed calculations of nanodisks with radii ranging from 19 to 29 nm on monolayer WS_2. Due to higher values of the dielectric function and a higher thickness of the multilayer WS_2, the LSPR of the nanodisks were red-shifted and the radii close to the excitonic resonance ranged from 11 to 21 nm. In all our calculations, we have used a thickness of 9 nm for the metallic core.[38] For the optical response of gold, we have used the dielectric function data reported by McPeak et al.,[55] to better reflect the single-crystalline nature of our nanodisks. We model the layer of CTAB molecule as a homogeneous 1 nm thick dielectric layer surrounding the nanodisks with a refractive index of 1.435.[63] The nanodisk with the CTAB layer was taken as being in direct contact with the WS_2. Both the single- and seven-layer WS_2 were modeled as homogeneous, isotropic bulk materials with effective thicknesses of 0.6 and 4.3 nm, respectively. The dielectric functions for both cases were extracted from experimental reflection measurements, followed by a treatment with the transfer-matrix method (see Tables S1 and S2). The SiO_2 substrate is modeled as a semi-infinite layer, and the dielectric function is taken from Malitson.[64] Moreover, for simplicity we have assumed that the exciting field is impinging at normal incidence onto the nanodisk. The scattering cross sections were evaluated by integrating the scattered energy density flowing through a surface with a radius of 100 nm and placed 150 nm above the nanodisk to simulate the numerical aperture of the objective used in our measurements (see Optical Measurements section). The absorption cross sections were calculated by integrating the energy density dissipated within the volume of the metallic core of the nanodisk and within the layered material WS_2 located below the nanodisk. The mesh size inside the WS_2 layers, the CTAB layer and in the metal core close to the metal/CTAB interface, were taken as small as 0.3 nm to allow numerical convergence. The remaining part of the nanodisks were meshed with elements with sizes ranging from 0.3 to 4 nm.

ASSOCIATED CONTENT

Supporting Information

The Supporting Information is available free of charge on the ACS Publications website at DOI: 10.1021/acsphotonics.8b01766.

Supporting figures and tables, as well as additional experimental details (PDF)

AUTHOR INFORMATION

Corresponding Author

*E-mail: niste@fotonik.dtu.dk.

ORCID

Mathias Geisler: 0000-0002-7764-2242
Jianfang Wang: 0000-0002-2467-8751
P. A. D. Gonçalves: 0000-0001-8518-3886
Peter Bøggild: 0000-0002-4342-0449
N. Asger Mortensen: 0000-0001-7936-6264
Sanshui Xiao: 0000-0001-6529-5047

DOI: 10.1021/acsphotonics.8b01766
ACS Photonics 2019, 6, 994−1001

Nicolas Stenger: 0000-0002-6808-9211

Notes

The authors declare no competing financial interest.

■ ACKNOWLEDGMENTS

We thank C. Tserkezis and J. M. Hvam for stimulating discussions. The Center for Nanostructured Graphene is sponsored by the Danish National Research Foundation (Project No. DNRF103). F.T. acknowledges a MULTIPLY fellowship under the Marie Skłodowska-Curie COFUND Action (Grant Agreement No. 713694) N.A.M. is a VILLUM Investigator supported by VILLUM FONDEN (Grant No. 16498). T.R. and A.B. acknowledge the IDUN Center of Excellence funded by the Danish National Research Foundation (Project No. DNRF122) and VILLUM FONDEN (Grant No. 9301).

■ REFERENCES

(1) Yoshie, T.; Scherer, A.; Hendrickson, J.; Khitrova, G.; Gibbs, H. M.; Rupper, G.; Ell, C.; Shchekin, O. B.; Deppe, D. G. Vacuum Rabi splitting with a single quantum dot in a photonic crystal nanocavity. *Nature* **2004**, *432*, 200−203.

(2) Wallraff, A.; Schuster, D. I.; Blais, A.; Frunzio, L.; Huang, R.-S.; Majer, J.; Kumar, S.; Girvin, S. M.; Schoelkopf, R. J. Strong coupling of a single photon to a superconducting qubit using circuit quantum electrodynamics. *Nature* **2004**, *431*, 162−167.

(3) McKeever, J.; Boca, A.; Boozer, A. D.; Buck, J. R.; Kimble, H. J. Experimental realization of a one-atom laser in the regime of strong coupling. *Nature* **2003**, *425*, 268−271.

(4) Marcos, D.; Wubs, M.; Taylor, J. M.; Aguado, R.; Lukin, M. D.; Sørensen, A. S. Coupling Nitrogen-Vacancy Centers in Diamond to Superconducting Flux Qubits. *Phys. Rev. Lett.* **2010**, *105*, 210501.

(5) Zhu, X.; Saito, S.; Kemp, A.; Kakuyanagi, K.; Karimoto, S.-i.; Nakano, H.; Munro, W. J.; Tokura, Y.; Everitt, M. S.; Nemoto, K.; Kasu, M.; Mizuochi, N.; Semba, K. Coherent coupling of a superconducting flux qubit to an electron spin ensemble in diamond. *Nature* **2011**, *478*, 221−224.

(6) Todisco, F.; De Giorgi, M.; Esposito, M.; De Marco, L.; Zizzari, A.; Bianco, M.; Dominici, L.; Ballarini, D.; Arima, V.; Gigli, G.; Sanvitto, D. Ultrastrong Plasmon-Exciton Coupling by Dynamic Molecular Aggregation. *ACS Photonics* **2018**, *5*, 143−150.

(7) Kamandar Dezfouli, M.; Tserkezis, C.; Mortensen, N. A.; Hughes, S. Nonlocal quasinormal modes for arbitrarily shaped three-dimensional plasmonic resonators. *Optica* **2017**, *4*, 1503.

(8) Törmä, P.; Barnes, W. L. Strong coupling between surface plasmon polaritons and emitters: a review. *Rep. Prog. Phys.* **2015**, *78*, 013901.

(9) Marquier, F.; Sauvan, C.; Greffet, J.-J. Revisiting Quantum Optics with Surface Plasmons and Plasmonic Resonators. *ACS Photonics* **2017**, *4*, 2091−2101.

(10) Baranov, D. G.; Wersäll, M.; Cuadra, J.; Antosiewicz, T. J.; Shegai, T. Novel Nanostructures and Materials for Strong Light-Matter Interactions. *ACS Photonics* **2018**, *5*, 24−42.

(11) Vasa, P.; Lienau, C. Strong Light-Matter Interaction in Quantum Emitter/Metal Hybrid Nanostructures. *ACS Photonics* **2018**, *5*, 2−23.

(12) Gonçalves, P. A. D.; Bertelsen, L. P.; Xiao, S.; Mortensen, N. A. Plasmon-exciton polaritons in two-dimensional semiconductor/metal interfaces. *Phys. Rev. B: Condens. Matter Mater. Phys.* **2018**, *97*, 041402.

(13) Fernández-Domínguez, A. I.; Bozhevolnyi, S. I.; Mortensen, N. A. Plasmon-Enhanced Generation of Nonclassical Light. *ACS Photonics* **2018**, *5*, 3447−3451.

(14) Groß, H.; Hamm, J. M.; Tufarelli, T.; Hess, O.; Hecht, B. Near-field strong coupling of single quantum dots. *Sci. Adv.* **2018**, *4*, No. eaar4906.

(15) Berrier, A.; Cools, R.; Arnold, C.; Offermans, P.; Crego-Calama, M.; Brongersma, S. H.; Gómez-Rivas, J. Active Control of the Strong Coupling Regime between Porphyrin Excitons and Surface Plasmon Polaritons. *ACS Nano* **2011**, *5*, 6226−6232.

(16) Zengin, G.; Wersäll, M.; Nilsson, S.; Antosiewicz, T. J.; Käll, M.; Shegai, T. Realizing Strong Light-Matter Interactions between Single-Nanoparticle Plasmons and Molecular Excitons at Ambient Conditions. *Phys. Rev. Lett.* **2015**, *114*, 157401.

(17) Chikkaraddy, R.; de Nijs, B.; Benz, F.; Barrow, S. J.; Scherman, O. A.; Rosta, E.; Demetriadou, A.; Fox, P.; Hess, O.; Baumberg, J. J. Single-molecule strong coupling at room temperature in plasmonic nanocavities. *Nature* **2016**, *535*, 127−130.

(18) Wersäll, M.; Cuadra, J.; Antosiewicz, T. J.; Balci, S.; Shegai, T. Observation of Mode Splitting in Photoluminescence of Individual Plasmonic Nanoparticles Strongly Coupled to Molecular Excitons. *Nano Lett.* **2017**, *17*, 551−558.

(19) Ramezani, M.; Halpin, A.; Fernández-Domínguez, A. I.; Feist, J.; Rodriguez, S. R.-K.; Garcia-Vidal, F. J.; Gómez Rivas, J. Plasmon-exciton-polariton lasing. *Optica* **2017**, *4*, 31.

(20) De Giorgi, M.; Ramezani, M.; Todisco, F.; Halpin, A.; Caputo, D.; Fieramosca, A.; Gomez-Rivas, J.; Sanvitto, D. Interaction and Coherence of a Plasmon-Exciton Polariton Condensate. *ACS Photonics* **2018**, *5*, 3666−3672.

(21) Wang, G.; Chernikov, A.; Glazov, M. M.; Heinz, T. F.; Marie, X.; Amand, T.; Urbaszek, B. Colloquium: Excitons in atomically thin transition metal dichalcogenides. *Rev. Mod. Phys.* **2018**, *90*, 021001.

(22) Liu, W.; Lee, B.; Naylor, C. H.; Ee, H.-S.; Park, J.; Johnson, A. T. C.; Agarwal, R. Strong Exciton-Plasmon Coupling in MoS_2 Coupled with Plasmonic Lattice. *Nano Lett.* **2016**, *16*, 1262−1269.

(23) Wang, S.; Li, S.; Chervy, T.; Shalabney, A.; Azzini, S.; Orgiu, E.; Hutchison, J. A.; Genet, C.; Samorì, P.; Ebbesen, T. W. Coherent Coupling of WS_2 Monolayers with Metallic Photonic Nanostructures at Room Temperature. *Nano Lett.* **2016**, *16*, 4368−4374.

(24) Liu, X.; Galfsky, T.; Sun, Z.; Xia, F.; Lin, E.-c.; Lee, Y.-H.; Kéna-Cohen, S.; Menon, V. M. Strong light-matter coupling in two-dimensional atomic crystals. *Nat. Photonics* **2015**, *9*, 30−34.

(25) Flatten, L. C.; He, Z.; Coles, D. M.; Trichet, A. A. P.; Powell, A. W.; Taylor, R. A.; Warner, J. H.; Smith, J. M. Room-temperature exciton-polaritons with two-dimensional WS_2. *Sci. Rep.* **2016**, *6*, 33134.

(26) Hu, T.; Wang, Y.; Wu, L.; Zhang, L.; Shan, Y.; Lu, J.; Wang, J.; Luo, S.; Zhang, Z.; Liao, L.; Wu, S.; Shen, X.; Chen, Z. Strong coupling between Tamm plasmon polariton and two dimensional semiconductor excitons. *Appl. Phys. Lett.* **2017**, *110*, 051101.

(27) Kleemann, M.-E.; Chikkaraddy, R.; Alexeev, E. M.; Kos, D.; Carnegie, C.; Deacon, W.; de Pury, A. C.; Große, C.; de Nijs, B.; Mertens, J.; Tartakovskii, A. I.; Baumberg, J. J. Strong-coupling of WSe_2 in ultra-compact plasmonic nanocavities at room temperature. *Nat. Commun.* **2017**, *8*, 1296.

(28) Han, X.; Wang, K.; Xing, X.; Wang, M.; Lu, P. Rabi Splitting in a Plasmonic Nanocavity Coupled to a WS_2 Monolayer at Room Temperature. *ACS Photonics* **2018**, *5*, 3970−3976.

(29) Tserkezis, C.; Gonçalves, P. A. D.; Wolff, C.; Todisco, F.; Busch, K.; Mortensen, N. A. Mie excitons: Understanding strong coupling in dielectric nanoparticles. *Phys. Rev. B: Condens. Matter Mater. Phys.* **2018**, *98*, 155439.

(30) Wen, J.; Wang, H.; Wang, W.; Deng, Z.; Zhuang, C.; Zhang, Y.; Liu, F.; She, J.; Chen, J.; Chen, H.; Deng, S.; Xu, N. Room-Temperature Strong Light-Matter Interaction with Active Control in Single Plasmonic Nanorod Coupled with Two-Dimensional Atomic Crystals. *Nano Lett.* **2017**, *17*, 4689−4697.

(31) Stührenberg, M.; Munkhbat, B.; Baranov, D. G.; Cuadra, J.; Yankovich, A. B.; Antosiewicz, T. J.; Olsson, E.; Shegai, T. Strong Light-Matter Coupling between Plasmons in Individual Gold Bi-pyramids and Excitons in Mono- and Multilayer WSe_2. *Nano Lett.* **2018**, *18*, 5938−5945.

(32) Cuadra, J.; Baranov, D. G.; Wersäll, M.; Verre, R.; Antosiewicz, T. J.; Shegai, T. Observation of Tunable Charged Exciton Polaritons

DOI: 10.1021/acsphotonics.8b01766
ACS Photonics 2019, 6, 994−1001

in Hybrid Monolayer WS_2-Plasmonic Nanoantenna System. *Nano Lett.* **2018**, *18*, 1777−1785.
(33) Wang, Q.; Sun, L.; Zhang, B.; Chen, C.; Shen, X.; Lu, W. Direct observation of strong light-exciton coupling in thin WS_2 flakes. *Opt. Express* **2016**, *24*, 7151.
(34) Yadgarov, L.; Višić, B.; Abir, T.; Tenne, R.; Polyakov, A. Y.; Levi, R.; Dolgova, T. V.; Zubyuk, V. V.; Fedyanin, A. A.; Goodilin, E. A.; Ellenbogen, T.; Tenne, R.; Oron, D. Strong light-matter interaction in tungsten disulfide nanotubes. *Phys. Chem. Chem. Phys.* **2018**, *20*, 20812−20820.
(35) Munkhbat, B.; Baranov, D. G.; Stührenberg, M.; Wersäll, M.; Bisht, A.; Shegai, T. Self-hybridized exciton-polaritons in multilayers of transition metal dichalcogenides for efficient light absorption. *ACS Photonics* **2019**, *6*, 139.
(36) Gong, S.-H.; Alpeggiani, F.; Sciacca, B.; Garnett, E. C.; Kuipers, L. Nanoscale chiral valley-photon interface through optical spin-orbit coupling. *Science* **2018**, *359*, 443−447.
(37) Chervy, T.; Azzini, S.; Lorchat, E.; Wang, S.; Gorodetski, Y.; Hutchison, J. A.; Berciaud, S.; Ebbesen, T. W.; Genet, C. Room Temperature Chiral Coupling of Valley Excitons with Spin-Momentum Locked Surface Plasmons. *ACS Photonics* **2018**, *5*, 1281−1287.
(38) Cui, X.; Qin, F.; Ruan, Q.; Zhuo, X.; Wang, J. Circular Gold Nanodisks with Synthetically Tunable Diameters and Thicknesses. *Adv. Funct. Mater.* **2018**, *28*, 1705516.
(39) Gutiérrez, H. R.; Perea-López, N.; Elías, A. L.; Berkdemir, A.; Wang, B.; Lv, R.; López-Urías, F.; Crespi, V. H.; Terrones, H.; Terrones, M. Extraordinary Room-Temperature Photoluminescence in Triangular WS_2 Monolayers. *Nano Lett.* **2013**, *13*, 3447−3454.
(40) Li, Y.; Chernikov, A.; Zhang, X.; Rigosi, A.; Hill, H. M.; van der Zande, A. M.; Chenet, D. A.; Shih, E.-M.; Hone, J.; Heinz, T. F. Measurement of the optical dielectric function of monolayer transition-metal dichalcogenides: MoS_2, $MoSe_2$, WS_2, and WS_2. *Phys. Rev. B: Condens. Matter Mater. Phys.* **2014**, *90*, 205422.
(41) Schuller, J. A.; Karaveli, S.; Schiros, T.; He, K.; Yang, S.; Kymissis, I.; Shan, J.; Zia, R. Orientation of luminescent excitons in layered nanomaterials. *Nat. Nanotechnol.* **2013**, *8*, 271−276.
(42) Ramasubramaniam, A. Large excitonic effects in monolayers of molybdenum and tungsten dichalcogenides. *Phys. Rev. B: Condens. Matter Mater. Phys.* **2012**, *86*, 115409.
(43) Jessen, B. S.; Whelan, P. R.; Mackenzie, D. M. A.; Luo, B.; Thomsen, J. D.; Gammelgaard, L.; Booth, T. J.; Bøggild, P. Quantitative optical mapping of two-dimensional materials. *Sci. Rep.* **2018**, *8*, 6381.
(44) Christiansen, D.; Selig, M.; Berghäuser, G.; Schmidt, R.; Niehues, I.; Schneider, R.; Arora, A.; de Vasconcellos, S. M.; Bratschitsch, R.; Malic, E.; Knorr, A. Phonon Sidebands in Monolayer Transition Metal Dichalcogenides. *Phys. Rev. Lett.* **2017**, *119*, 187402.
(45) Gonçalves, P. A. D.; Peres, N. M. R. *An Introduction to Graphene Plasmonics*; World Scientific: Singapore, 2016.
(46) Zhan, T.; Shi, X.; Dai, Y.; Liu, X.; Zi, J. Transfer matrix method for optics in graphene layers. *J. Phys.: Condens. Matter* **2013**, *25*, 215301.
(47) Qin, F.; Zhao, T.; Jiang, R.; Jiang, N.; Ruan, Q.; Wang, J.; Sun, L.-D.; Yan, C.-H.; Lin, H.-Q. Thickness Control Produces Gold Nanoplates with Their Plasmon in the Visible and Near-Infrared Regions. *Adv. Opt. Mater.* **2016**, *4*, 76−85.
(48) Wang, F.; Shen, Y. R. General Properties of Local Plasmons in Metal Nanostructures. *Phys. Rev. Lett.* **2006**, *97*, 206806.
(49) Flick, J.; Rivera, N.; Narang, P. Strong light-matter coupling in quantum chemistry and quantum photonics. *Nanophotonics* **2018**, *7*, 1479−1501.
(50) Wu, X.; Gray, S. K.; Pelton, M. Quantum-dot-induced transparency in a nanoscale plasmonic resonator. *Opt. Express* **2010**, *18*, 23633.
(51) Cong, C.; Shang, J.; Wang, Y.; Yu, T. Optical Properties of 2D Semiconductor WS_2. *Adv. Opt. Mater.* **2018**, *6*, 1700767.
(52) Antosiewicz, T. J.; Apell, S. P.; Shegai, T. Plasmon-Exciton Interactions in a Core-Shell Geometry: From Enhanced Absorption to Strong Coupling. *ACS Photonics* **2014**, *1*, 454−463.
(53) Yorulmaz, M.; Nizzero, S.; Hoggard, A.; Wang, L.-Y.; Cai, Y.-Y.; Su, M.-N.; Chang, W.-S.; Link, S. Single-Particle Absorption Spectroscopy by Photothermal Contrast. *Nano Lett.* **2015**, *15*, 3041−3047.
(54) This shift is predicted from Mie theory and has also been demonstrated experimentally.[53]
(55) McPeak, K. M.; Jayanti, S. V.; Kress, S. J. P.; Meyer, S.; Iotti, S.; Rossinelli, A.; Norris, D. J. Plasmonic Films Can Easily Be Better: Rules and Recipes. *ACS Photonics* **2015**, *2*, 326−333.
(56) Olmon, R. L.; Slovick, B.; Johnson, T. W.; Shelton, D.; Oh, S.-H.; Boreman, G. D.; Raschke, M. B. Optical dielectric function of gold. *Phys. Rev. B: Condens. Matter Mater. Phys.* **2012**, *86*, 235147.
(57) Johnson, P. B.; Christy, R. W. Optical Constants of the Noble Metals. *Phys. Rev. B* **1972**, *6*, 4370−4379.
(58) Yakubovsky, D. I.; Arsenin, A. V.; Stebunov, Y. V.; Fedyanin, D. Y.; Volkov, V. S. Optical constants and structural properties of thin gold films. *Opt. Express* **2017**, *25*, 25574.
(59) Wang, S.; Le-Van, Q.; Vaianella, F.; Maes, B.; Eizagirre Barker, S.; Godiksen, R. H.; Curto, A. G.; Gomez Rivas, J. Limits to Strong Coupling of Excitons in Multilayer WS2 with Collective Plasmonic Resonances. *ACS Photonics* **2019**, *6*, 286−293.
(60) Zheng, D.; Zhang, S.; Deng, Q.; Kang, M.; Nordlander, P.; Xu, H. Manipulating Coherent Plasmon-Exciton Interaction in a Single Silver Nanorod on Monolayer WSe_2. *Nano Lett.* **2017**, *17*, 3809−3814.
(61) Bisht, A.; Cuadra, J.; Wersäll, M.; Canales, A.; Antosiewicz, T. J.; Shegai, T. Collective Strong Light-Matter Coupling in Hierarchical Microcavity-Plasmon-Exciton Systems. *Nano Lett.* **2019**, *19*, 189.
(62) Sáez-Blázquez, R.; Feist, J.; Fernández-Domínguez, A. I.; García-Vidal, F. J. Enhancing photon correlations through plasmonic strong coupling. *Optica* **2017**, *4*, 1363.
(63) Kekicheff, P.; Spalla, O. Refractive Index of Thin Aqueous Films Confined between Two Hydrophobic Surfaces. *Langmuir* **1994**, *10*, 1584−1591.
(64) Malitson, I. H. Interspecimen Comparison of the Refractive Index of Fused Silica. *J. Opt. Soc. Am.* **1965**, *55*, 1205.

DOI: 10.1021/acsphotonics.8b01766
ACS Photonics 2019, 6, 994−1001